Passivity-based control for flux regulation in a variable reluctance finger gripper

K.K. Chan, J.M. Yang and N.C. Cheung

Abstract: A flux regulation method with passivity-based control (PBC) for a variable reluctance (VR) finger gripper is presented. The performance and stability of the proposed control scheme is verified through mathematical derivations and computer simulation. These verifications indicate that the direct-drive VR finger gripper control has robustness despite certain parameters variations and modelling uncertainties. A novel two-finger gripper based on VR driving principle is also introduced. This kind of gripper has certain advantages over the conventional permanent magnet voice coil gripper, the most notable advantages are the ease of construction, high robustness and very low cost. The work described is the first of its kind in carrying out passivity based control for a direct-drive VR actuator. In the study, the flux and torque behaviour of a mutually-coupled VR gripper was investigated, and its state dynamic equations were derived. Then its flux and torque models were constructed. A similar two-finger VR gripper was fabricated and its characteristics were measured. The PBC controller is designed to regulate the flux linking through the magnetic circuit of the VR finger gripper. Computer simulation and hardware implementation were carried out. The two sets of results compare favourably with each other. Both sets of result show that the system is highly robust and has excellent trajectory tracking performance.

1 Introduction

The variable reluctance (VR) motor has drawn much research attention over the past decade, because of its robustness and low-cost structure, and its potential for numerous industrial applications. However, the VR motor has inherent nonlinear characteristics; problems of torque-ripple and non-uniform force occur when it is driven by standard motor drives [1]. During the past few years, many publications on VR motor design, commutation methods and VR motor drives have emerged. These methods were made possible by the advancement of simulation tools and computer control technologies. Now, it is possible to accommodate most of the nonlinear side-effects into the construction and simulation of the VR motor model, and into the real-time control of the VR motor.

To convert the nonlinear actuator into a proportional device, researchers have developed numerous ideas and adopted various control algorithms to solve the problem. The most common method is to use lookup tables for the nonlinear torque compensation [2]. This method involves little computation, but it is costly in terms of memory storage. The cost can be lowered by reducing the size of the lookup table with first-or second-order interpolation [3]. However, this method introduces extra error to the system. With the dramatic increase in the processing power of digital signal processors (DSP) and reduction in price of these components, advanced control algorithms can be employed even though there is limited memory size, and thus various control algorithms have emerged. Modern control strategies like fuzzy logic have been employed. They can deal with the nonlinearity problem and have adaptive capability for torque ripple minimisation [4, 5]. These strategies do not require a full mathematical description of the target plant. However, some successful simulation and experiment examples using non-model based intelligent control methods are lacking in proofs on the control stability. They cannot guarantee global system stability, consistent performance and high robustness for all operating conditions.

PBC is a controller design approach with 'energy-shaping'. PBC yields a closed-loop energy that is equal to the difference between the stored and the supplied energies, namely energy-balancing [6]. When a passivity-based controller is designed a desired energy function is first selected. Then the controller can be designed to ensure this objective. This energy-balancing property is clearly a universal property of passive physical systems, including nonlinear and time-varying ones. With the presence of dissipation, the energy of the system is clearly non-increasing, thus the rate of convergence of the energy function can be increased by increasing the system damping through some means of control, namely damping injection. The attractive features of this approach are the enhanced robustness and the lack of controller calculation singularities. These properties are based on the fact that cancellation of system nonlinear terms is avoided through PBC.

In this paper, a PBC strategy is adopted and a nonlinear flux controller of the VR finger gripper is developed. The VR finger gripper model is presented in the port-controlled Hamiltonian model, which encompasses a very large class of physical nonlinear systems. It provides a classification of the variables and the equations into those associated with the phenomenological properties and those defining the interconnection structure related to the exchanges of energy. Therefore, they are well-suited to carry out the basic steps

IEE Proceedings online no. 20040318

doi:10.1049/ip-epa:20040318

Paper first received 6th June and in revised form 26th November 2003. Originally published online: 8th April 2005

K.K. Chan and N.C. Cheung is with the Department of Electrical Engineering, Hong Kong Polytechnic University, Hung Hom, Hong Kong

J.M. Yang is with the Electrical Power College, South China, University of Technology, Guangzhou 510640, People's Republic of China

of PBC of modifying the energy function and damping injection. The PBC is designed by reshaping the system's natural energy and injecting the required damping to achieve the control objective [7]. The proposed control scheme guarantees the global asymptotic stability and system robustness in response to some plant variations and modelling uncertainties. In recent years, the PBC strategy has been adopted by power electronics researchers to solve various problems in areas such as power converters, power factor compensators and electric motor control [8–10].

The work described in this paper show that the model of VR finger gripper is accurate and the proposed PBC can be an effective solution for the control of the VR finger gripper.

2 Proposed structure of the VR gripper

Figure 1 shows the structure of the two-finger VR gripper. It consists of two rotary elements, each attached to a finger. The stator contains two coils, each with a 400-turn winding. The moving rotors are mounted on two individual shafts, whose axes are normal to the plane of the diagram. The moving elements may rotate freely between the poles of the stator. Both the rotors and stators are made up of laminated mild steel to reduce eddy currents.

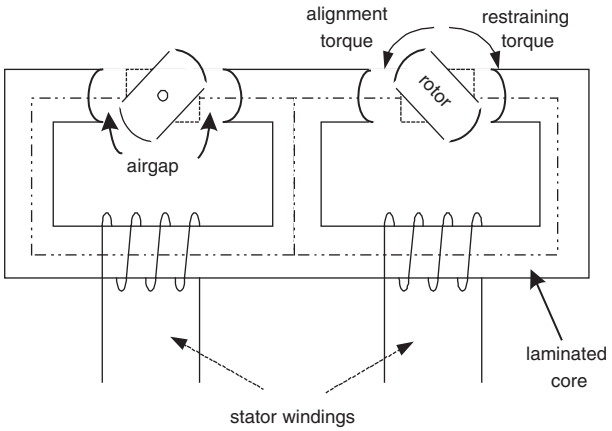

Fig. 1 *Proposed VR finger gripper*

The two fingers of the gripper are 90 mm long and are preloaded with torsion springs. This arrangement allows bidirectional movements from a single-direction coil excitation. When currents are applied to the stator windings, the rotors will rotate away from their initial rest positions with a tendency to reduce their reluctance by torque alignment. The rotors will stop when alignment torques comes into equilibrium with restraining torques provided by the springs. When the fingers rotate by 70°, the fingertips will be fully closed. For each rotating axis, there is an incremental rotary encoder with a resolution of 0.09° connected onto the rotating shaft to measure the rotor position.

Figure 2 shows the construction of the VR gripper at (*a*) grasp and (*b*) release positions, respectively. Figures 3*a* and *b* show the spring characteristics and its linearity measurement, respectively. In this case, the springs are assumed to be linear with worst case error around 5%. The overall construction is extremely simple and robust, and it is very similar to the rotary solenoids, which use simple on–off mechanical actuation devices. Combining the two fingers into a single magnetic housing has made the finger alignment process much simpler and the overall size much smaller.

3 VR finger gripper model

The electrical behavior of the VR gripper can be expressed as:

$$v = R_m i + \frac{d\lambda}{dt} \tag{1}$$

where v is the voltage applied across the stator winding, R_m is the stator winding resistance, λ is the flux linkage and θ is the rotor position. This can be further expanded into:

$$v = R_m i + \frac{\partial\lambda}{\partial i}\frac{di}{dt} + \frac{\partial\lambda}{\partial\theta}\frac{d\theta}{dt} \tag{2}$$

The instantaneous torque production, T, of the VR gripper is given by:

$$T = \left[\frac{\partial W_c}{\partial\theta}\right]_{i=\text{const}} \tag{3}$$

where θ is the angular position of the rotor, i is the stator current and W_c is the co-energy, which can be

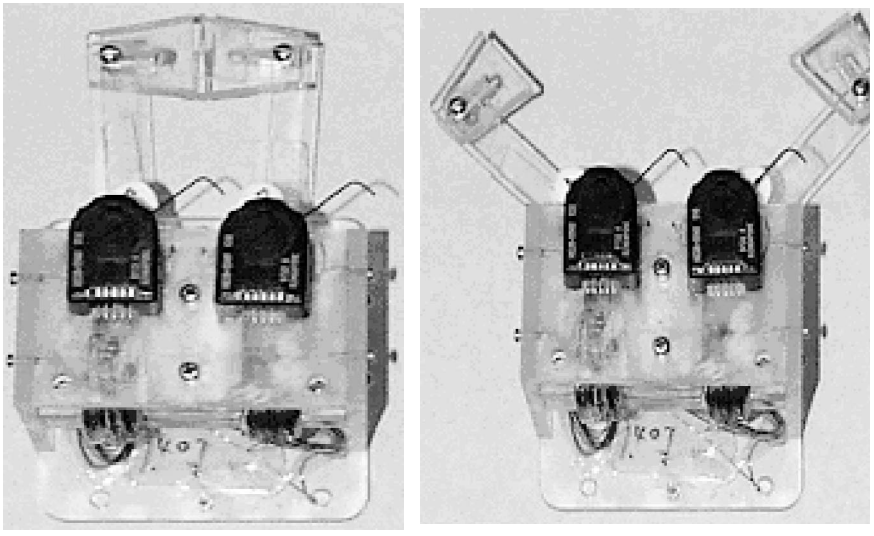

a *b*

Fig. 2 *VR finger gripper*
a At grasp position
b At release position

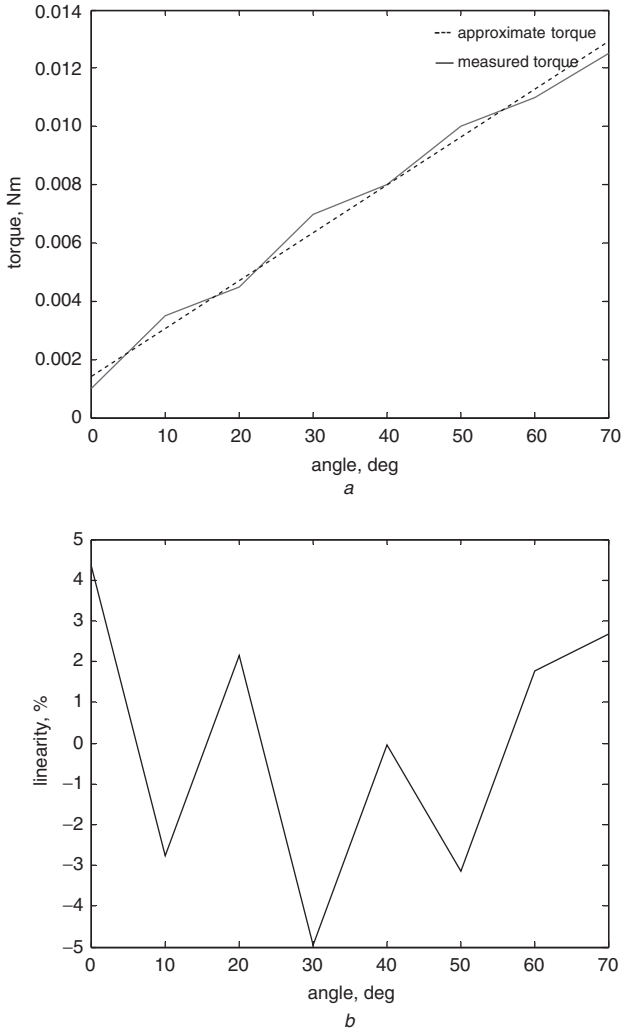

Fig. 3 *Spring torque characteristic*
a Measured torque and approximate torque
b Linearity plot

expressed as [1]:

$$W_c = \int_0^i \lambda di \tag{4}$$

It is important to notice that there is stroke limit of 70° for the VR finger gripper, which prevents the rotor from achieving extremely high speed. In other words, the current loop response is much faster than the mechanical one. As a result, by combining (3) and (4), the torque production can be approximated as:

$$T \approx i\frac{\partial \lambda}{\partial \theta} \tag{5}$$

The state dynamic equation of the VR finger gripper can be represented as:

$$J_m\ddot{\theta} = -K_{sp}\theta - K_v\ddot{\theta} + T - T_L \tag{6}$$

where J_m is the total rotor and load inertia, K_{sp} is the spring constant, K_v is the viscous damping constant and T_L is the load torque required. If the magnetic circuit is pseudo-linear, the inductance profile may be described by using the first two terms of the Fourier series approximation [11, 12]

$$L(\theta) = L_0 + L_1\cos(\theta) \tag{7}$$

Note that the VR finger gripper should not only have the fundamental components but also possess higher harmonic components; however the model would become very difficult to solve and to derive a controller mathematically from a system stability perspective. With the above assumption, the controller must acquire a certain degree of stability robustness to maintain its stability.

4 Passivity-based control and port-controlled Hamiltonian model

The state vector, x is chosen as $x = [Li\ K_{sp}\theta\ J_m\dot{\theta}]^T$

The total energy function, $H(x)$ can be defined as the sum of the electromagnetic stored energy and kinetic energy, and stored spring potential energy:

$$H(x) = \frac{1}{2}\left(Li^2 + K_{sp}\theta^2 + J\dot{\theta}^2\right) \tag{8}$$

With this energy function, the model of the VR finger gripper given in (1) and (2) can be rearranged as the equation of the port-controlled Hamiltonian (PCH) [7]:

$$\dot{x} = [J(x) - R]\frac{\partial H(x)}{\partial x} + g \cdot u + \xi \tag{9}$$

where J is a skew symmetric matrix, R is a positive definite matrix, g is the input voltage vector and ξ is the disturbance vector. R represents the dissipative elements and must be positively defined, otherwise the energy stored within the system will not be less than the energy supplied into the system. Under this situation, the system will not be a passivity system. Using (1), (2) and the selected state vector, x, the dynamic model in PCH format can be represented as:

$$\dot{x} = \left\{ \begin{bmatrix} 0 & 0 & \frac{\partial \lambda}{\partial \theta} \\ 0 & 0 & K_{sp} \\ \frac{\partial \lambda}{\partial \theta} & -K_{sp} & 0 \end{bmatrix} - \begin{bmatrix} R_m & 0 & 0 \\ 0 & K & 0 \\ 0 & 0 & K_v \end{bmatrix} \right\} D^{-1}x + \begin{bmatrix} 1 \\ 0 \\ 0 \end{bmatrix} u + \begin{bmatrix} 0 \\ \frac{K}{K_{sp}}x^2 \\ -T_L \end{bmatrix} \tag{10}$$

$$\text{where } D^{-1} = \begin{bmatrix} \frac{1}{L} & 0 & 0 \\ 0 & \frac{1}{K_{sp}} & 0 \\ 0 & 0 & \frac{1}{J} \end{bmatrix}$$

In this context, K is a positive number and it is artificially inserted into the equation to maintain the positive definiteness of R. However, with the natural dissipative elements of the actual plant, the system damping will be small and it will reduce the closed loop system performance. Additional damping injection is required. It can be achieved by inserting an additional constant, K' into the dissipative matrix, R, as shown by:

$$\dot{x} = \left\{ \begin{bmatrix} 0 & 0 & -\frac{\partial \lambda}{\partial \theta} \\ 0 & 0 & K_{sp} \\ \frac{\partial \lambda}{\partial \theta} & -K_{sp} & 0 \end{bmatrix} - \begin{bmatrix} R_m & 0 & 0 \\ 0 & K & 0 \\ 0 & 0 & K_v + K' \end{bmatrix} \right\} D^{-1}x + \begin{bmatrix} 0 \\ \frac{K}{K_{sp}}x_2 \\ \frac{K'}{J}x_3 - T_L \end{bmatrix} + \begin{bmatrix} 1 \\ 0 \\ 0 \end{bmatrix} u \tag{11}$$

5 Passivity-based controller design

The state error can be defined as $e = x - x_d$, where x_d is the reference state vector, which defines the desired system

performance. Substituting $e = x - x_d$ into (2), the model of the state error becomes:

$$\dot{e} + [R - J]D^{-1}e = \phi \tag{12}$$

where $\phi = -\dot{x}_d + [J - R]D^{-1}x_d + gu + \zeta$. According to Lyapunov stability criteria [13], the scalar function $V(x)$ representing the system energy must posess the following properties.

$V(0) = 0$;

$V(x) > 0, ||x|| \neq 0$;

V is continuous and has continuous derivatives with respect to all components of x

$\dot{V}(x) \leq 0$ along trajectories of the equation.

This control problem is defined as a trajectory problem. The system energy function, $V(x)$, can be defined as:

$$V = \frac{1}{2}e^T D^{-1} e \tag{13}$$

where e represents the trajectory error.

Therefore:

$$\begin{aligned}\dot{V} &= e^T D^{-1}\dot{e} \\ &= c^T D^{-1}[(J - R)D^{-1}e + \phi] \\ &= e^T D^{-1} J D^{-1} e - e^T D^{-1} R D^1 e + e^T D^{-1}\phi\end{aligned} \tag{14}$$

From (14), $e^I D^{-1} J D^{-1} e$, the first term, consists of a matrix J, which is skew-symmetric and clearly becomes zero. It imposes no action on stability and is called a 'workless force'. The second term, $-e^{\tau} D^{-1} J D^{-1} e$, has matrix R and D^{-1} which are both positive definite and make the entire term negative. In order to maintain the system stability in the Lyapunov sense, ϕ needs to be zero through suitable control effort, which yields $\dot{V} = -e^T D^{-1} R D^{-1} e$. The state error system is asymptotically stable. Furthermore, the state error converges exponentially, i.e. $|e| < k_0 e^{-\mu 0}|e(0)|$, where k_0 and μ_0 are positive scalars. In addtiton, (12) shows that, for tracking problem, $\dot{e} = e = 0$ and $\phi = 0$ is a correct choice. Furthermore, system stability can still be preserved to some extent despite of the presence of certain parameters variations. This is because parameter variations in λ, for example introduced through unmodelled hystersis effect and K_{sp}, still maintain the skew-symmetric property in matrix J. Similarly, variations in R_m and K_v do not influence the positive definiteness of matrix R. Such a property ensures that the system can automatically preserve a certain robustness.

Expanding (14) with $\phi = 0$, three differential equations can be obtained:

$$-\dot{x}_{d1} - \frac{1}{J}\frac{\partial \lambda}{\partial \theta}x_{d3} - \frac{R_m}{L}x_{d1} + u = 0 \tag{15}$$

$$-\dot{x}_{d2} + \frac{1}{J}K_{sp}x_{d3} - \frac{K}{K_{sp}}x_{d2} + \frac{K}{K_{sp}}x_2 = 0 \tag{16}$$

$$\begin{aligned}-\dot{x}_{d3} + \frac{1}{L}\frac{\partial \lambda}{\partial \theta}x_{d1} - x_{d2} - \frac{(K_v + K')}{J}x_{d3} + \frac{K'}{J}x_3 - T_L \\ = 0\end{aligned} \tag{17}$$

Rearranging in terms of x_{d2}, (16) becomes:

$$x_{d3} = \frac{J}{K_{sp}}\left(\dot{x}_{d2} + \frac{K}{K_{sp}}x_{d2} - \frac{K}{K_{sp}}x_2\right) \tag{18}$$

By substituting (18) into (17), (17) becomes a second order differential equation:

$$\begin{aligned}&\ddot{x}_{d2} + \left[\frac{K}{K_{sp}} + \frac{(K_v + K')}{J}\right]\dot{x}_{d2} + \left[\frac{K_{sp}}{J} + \frac{(K_v + K')}{J}\frac{K}{K_{sp}}\right]x_{d2} \\ &= \frac{K}{K_{sp}}\dot{x}_2 + \frac{K_{sp}}{J}\frac{i}{L}\frac{\partial L}{\partial \theta}x_{d1} + \frac{(K_v + K')}{J}\frac{K}{K_{sp}}x_2 \\ &\quad + \frac{K_{sp}}{J}\frac{K'}{J}x_3 - \frac{K_{sp}}{J}T_L\end{aligned} \tag{19}$$

As a result, valid sets of K and K' can be determined by equating the coefficients of a general second-order differential equation:

$$\frac{K}{K_{sp}} + \frac{(K_v + K')}{J} = 2\xi\omega_n \tag{20}$$

$$\frac{K_{sp}}{J} + \frac{(K_v + K')}{J}\frac{K}{K_{sp}} = \omega_n^2 \tag{21}$$

Solving (20) and (21) with quadratic equations and selecting ξ and ω_n as 1 and 700rad/s, K and K' can be calculated as 6 and 1 respectively. Classically, it is common to choose $\xi = 0.7$. However, to prevent the two-VR gripper from experiencing any mechanical overshoot and introducing a high impact force onto the target object, $\xi = 1$ is chosen. Similarly, w_n is chosen in such a way that the controller would have a high closed-loop bandwidth while not exciting system resonance.

Note that the rate of change of current falls to zero at steady state and thus $\dot{x}_{d1} = 0$. The control law (15) becomes:

$$u = \frac{R_m}{L}x_{d1} + \frac{1}{J}\frac{\partial \lambda}{\partial \theta}x_{d3} \tag{22}$$

System output damping can be further increased without altering the control law and affecting the stability. The alterations can be made at the command input, using the following command shaping:

$$x_{d1}\prime = x_{d1} - K''\dot{\theta} \tag{23}$$

After command shaping, x_{d1} becomes the system reference input and x_1 becomes the flux linkage estimated output. The PBC controller takes x_{d3} as feedback, which is obtained by solving (18) and (19) for current and angular velocity.

6 Determining the flux profile

From the formulated model, most parameters can be obtained through either calculation or experimental measurement. Apart from flux linkage λ, all the parameters are given in Table 1. However, for the VR finger gripper, flux linkage measurement requires a special technique [1].

Rearranging (1), flux linkage, λ can be obtained as:

$$\lambda = \int (v - R_m i)dt \tag{24}$$

A step voltage can be injected into the stator windings, which are connected in series to ensure that the current flows through both windings are equal. Figure 4 shows the circuit diagram for the flux linkage measurement setup. Note that the switch used was a solid-state switch instead of a classical mechanical switch, which would introduce unnecessary mechanical bouncing and disturb the input voltage applied across the stator windings. In contrast, the solid-state switch offers fast switching response and is vibration free. This method was further improved by

Table 1: VR gripper profile

	Notation	Values	
Rotor inertia	J_m	0.1	mNm
Spring constant	K_{sp}	0.01	Nm/rad
Viscous constant	K_v	10^{-3}	Nm/rad/s
Resistance of stator winding	R_m	4	Ω
Number of turns in stator winding	N	400	turns
Max. continuous current	I	4	A

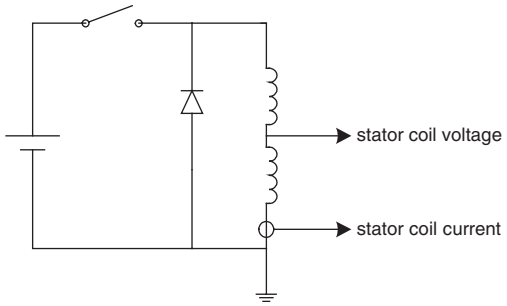

Fig. 4 *Circuit diagram for flux linkage measurement setup*

employing a lead–acid battery as the voltage source [14]. This can completely eliminate current ripples due to RLC oscillations.

A dSPACE DS1104 card was used as the data acquisition controller. The card had an on-board 250 MHz MPC8240, PowerPC 603e core for real-time computation and it interfaced with the PC through the PCI bus. It consists of two 24-bit digital incremental encoder input channels, four 16-bit ADCs and seven PWM channels. By connecting with Matlab real-time workshop and Simulink, real-time control C-code can be generated with a Simulink diagram. Assembly codes can be compiled and downloaded to the DSP. Voltages applied across, and currents flowing through, the stator windings were fed into the ADC channels. Encoders were also connected to the measurement system to provide high-precision position information. The two fingers were fixed with a fixture at the same rotational angle. Results were measured with angular positions from 0 to 70° and current levels from 0 to 7A.

Using (24), flux can be determined and Fig. 5*a* shows the flux characteristic profile of the VR finger gripper at different rotor angles from unaligned to fully aligned positions. Figure 5*b* shows the 3D flux profile of the VR finger gripper. Below a current 2A, the actuator works within the linear region.

7 Simulation

As the experiment will be implemented onto the dSPACE system (see section 6), certain simulation settings need to be matched with the actual hardware to obtain an accurate simulation result. The simulation of the PBC controller was done using Matlab Simulink. The controller needs to be, on the one hand, fast in dynamics but, on the other hand, robust enough to stay stable within the entire load variation range. Slight oscillations can be amplified mechanically and exhibited onto the finger tip and deteriorate the entire system performance. Thus, a 5 kHz sampling rate selected.

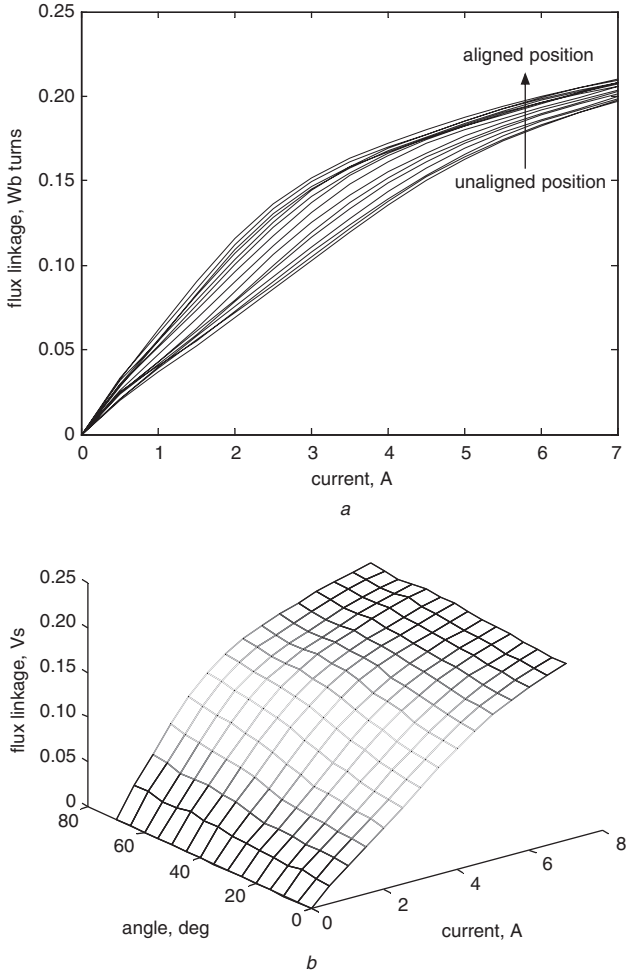

Fig. 5 *Flux linkage profile*
a At different rotor angles
b 3D flux characteristic profile

To solve the differential equations, an integration solver using the Euler numerical method was employed. The same method was selected for the actual hardware implementation.

In the simulation, a step flux linkage input of 0.1 Wb.turns with a period of one second and 80% duty cycle was injected into the simulation model. Figures. 6*a* and *b* show the simulation results for state responses and the corresponding tracking errors. Figure 6 shows that all states have fast tracking responses. Peak time of x_1 was 30 ms, and the mechanical tracking error for x_2 and x_3 settle within 100 ms. Simulation results show that the controlled system is stable and offers fast tracking responses.

8 Implementation and results

Apart from the PBC controller, another controller was also implemented, which served as a comparison. The other flux-linkage controller was calculated from the current reference using a predetermined lookup table comprising 15 different current levels and 15 different rotary positions, with intermediate values obtained through linear interpolation. It requires position information feedback such that it can effectively determine the required current level since flux linkage varies as the rotor stays at different positions. Figure 7 shows the block diagram for the implementations of both controllers.

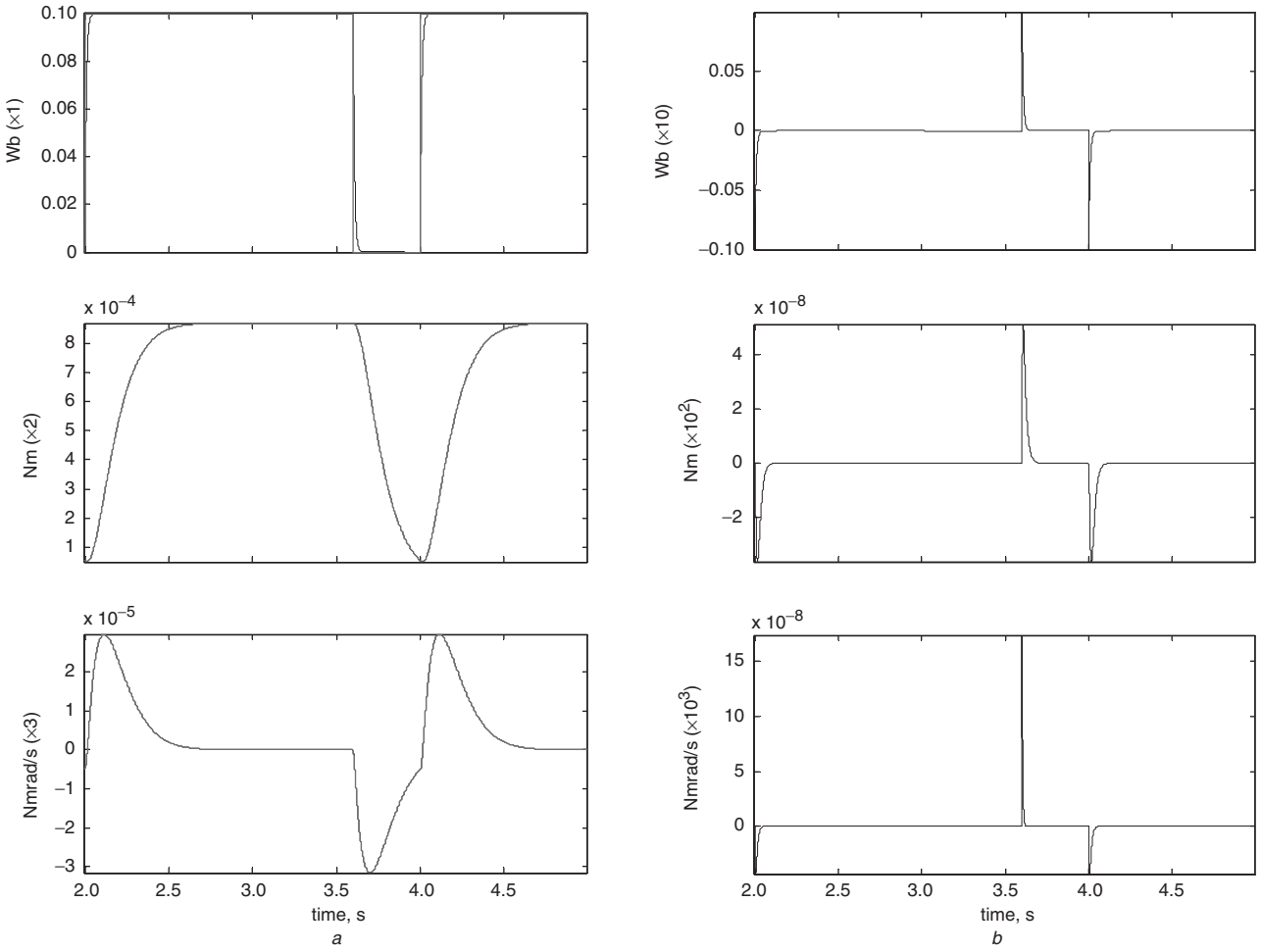

Fig. 6 *Simulation results*
a Tracking responses of each state
b Tracking error of each state

Each controller was implemented digitally using the data acquisition system mentioned in Section 6. For both cases, the VR finger gripper was driven by a switching power stage. This switching power stage converts controlled PWM signals into the PWM high voltage source and excites the stator coils. The conditioned current signal and encoder position was sampled by the controller for the calculation of the next controlled signal. Figure 8 shows the schematic block diagram of the switching power stage used in this project.

The PWM driver used in the project was a pair of high-low side power MOSFETs, IRF740, half-bridge amplifiers. It acted as a current amplifier for the motor. It has fewer components than the full bridge amplifier and has a true ground that makes current measurement much simpler. The current feedback circuit had a gain of 1.2 A/V. The motor side and logic side were electrically isolated by the opto-couplers that introduced about a 300 ns delay. Dead-time delay protection against cross conduction of the high-low side MOSFETs was introduced. The chopping frequency was set at 24 kHz to ensure good current dynamics and minimal current ripple.

Initially, the VR finger was at open positions. Then a step input flux linkage command of 0.04 Wb.turns, which is equivalent to around 1A current, was injected into both controllers. Figure 9 shows the measured stator current responses for both PBC and lookup-table flux-linkage controllers. It is clearly shown that, for the step response of PBC controller, there was a much smaller overshoot compared with the lookup-table method. The response of PBC controller had a peak and settling time of 0.095 and 0.14s, whereas while the lookup-table method had a peak and settling time of 0.1 and 0.15s, respectively. It is clear that the PBC controller enjoys a faster response in both rise time and settling time than its counterpart.

Figure 10 shows the experimental trajectory response and error for each state variable with a flux-linkage of 0.15 Wb.turns. For this case, a high level of step command would introduce large excitation into the system and thus increase settling time and tracking error. As an result, a S-curve profile was employed to reduce the input command bandwidth. The equation can be expressed as:

$$\lambda_{\text{cmd}} = \frac{t}{t + e^{(c1 - c2t)}} \tag{25}$$

where λ_{cmd}, t, $c1$ and $c2$ represent flux-linkage command, time and constants for shaping the curve. Command shaping mentioned (23) is also employed to reduce the mechanical vibrations for x_2 and x_3. Results show that all states are stable and converge asymptotically. The worst case dynamic errors for x_1, x_2 and x_3 are 0.06 Wbturns, 0.5 mNm and 0.02 mNmrad/s.

Figure 11 shows experimental trajectory response and error for each state variable with the spring constant doubled. As shown clearly from the results the system still remains stable and exhibits asymptotic convergence. With the spring constant doubled, the mechanical bandwidth is also increased with higher rigidity. System responses show

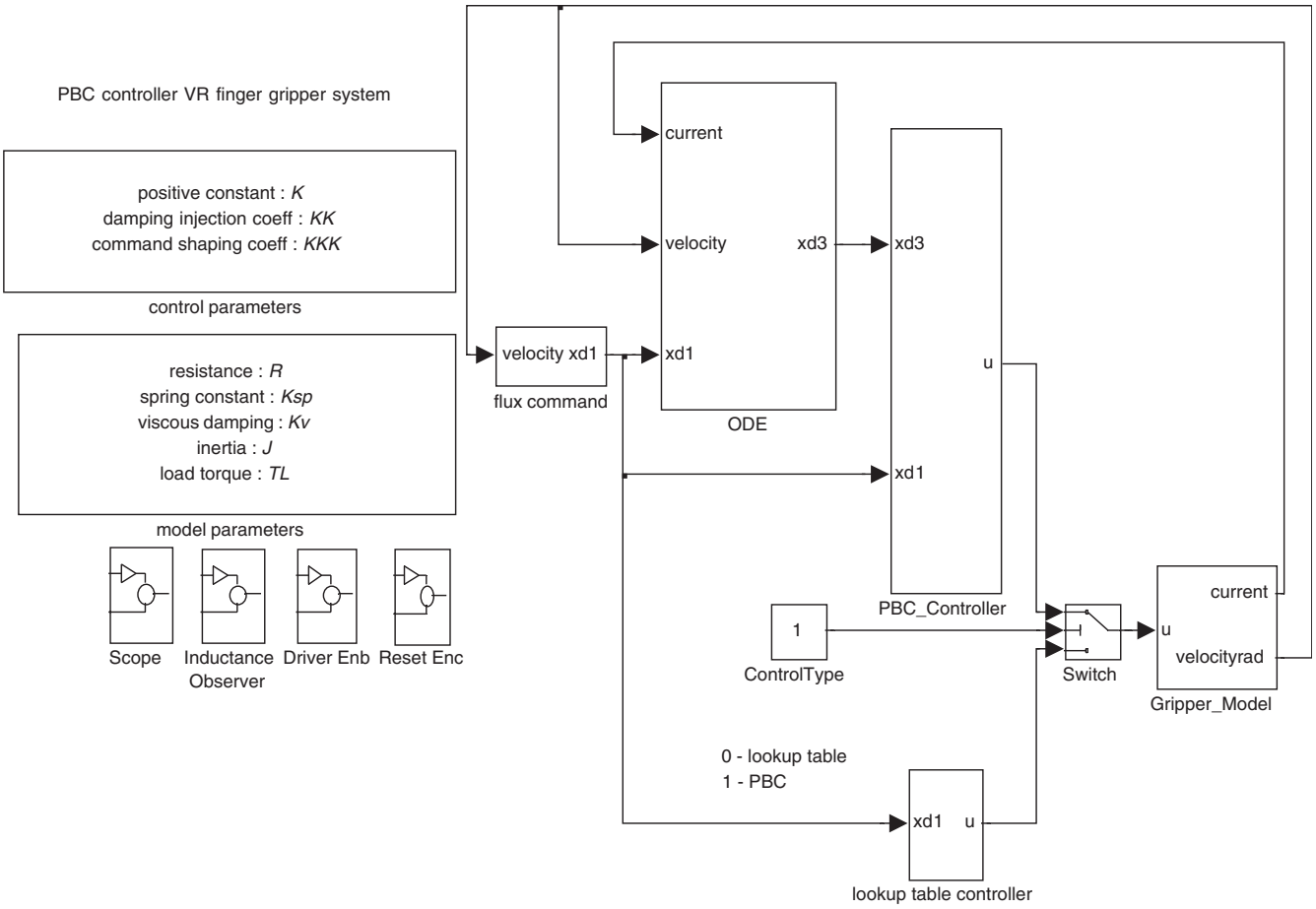

Fig. 7 *Block diagram of a PBC controller for the VR finger gripper*

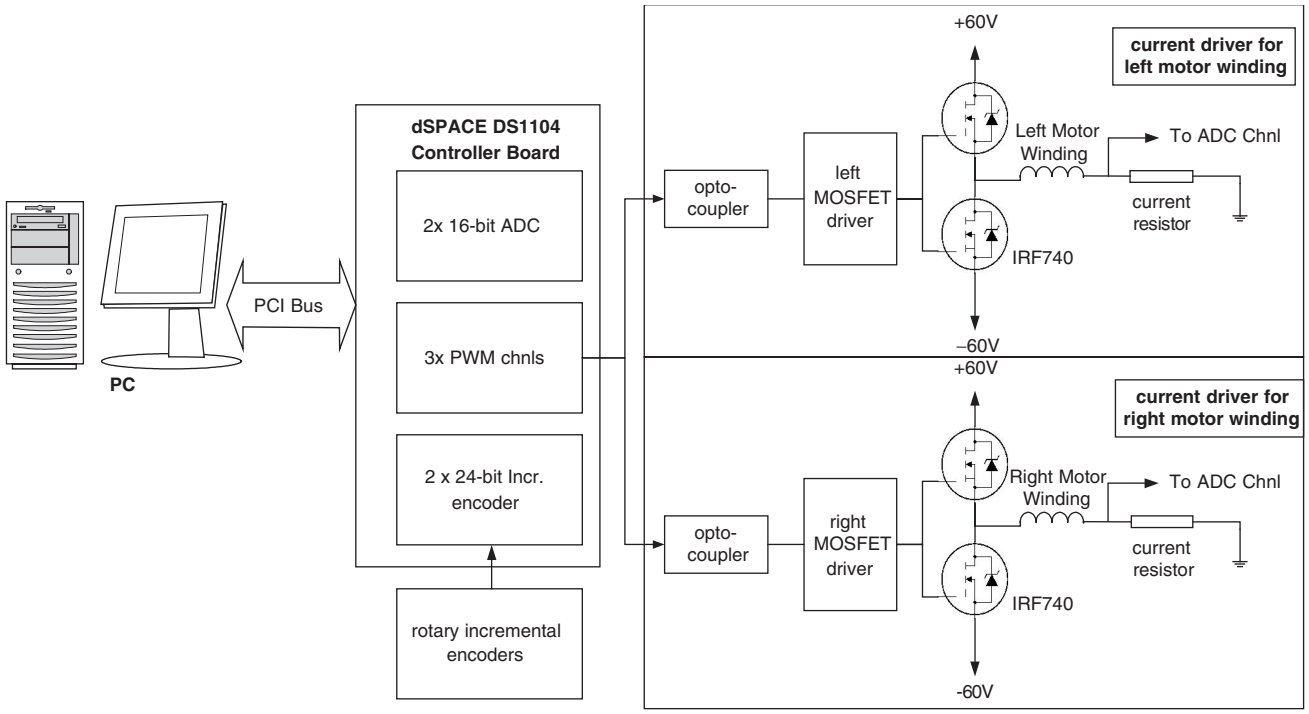

Fig. 8 *Schematic block diagram of a half-bridge amplifier for the VR finger gripper*

higher frequency components and thus have smaller dynamic tracking error. Here, the worst case dynamic errors for x_1, x_2 and x_3 are 0.04 Wbturns, 0.4 mNm and 0.02 mNmrad/s.

The experimental results show that the proposed passivity-based controller for flux regulation for the variable reluctance finger gripper is stable, robust and has high performance.

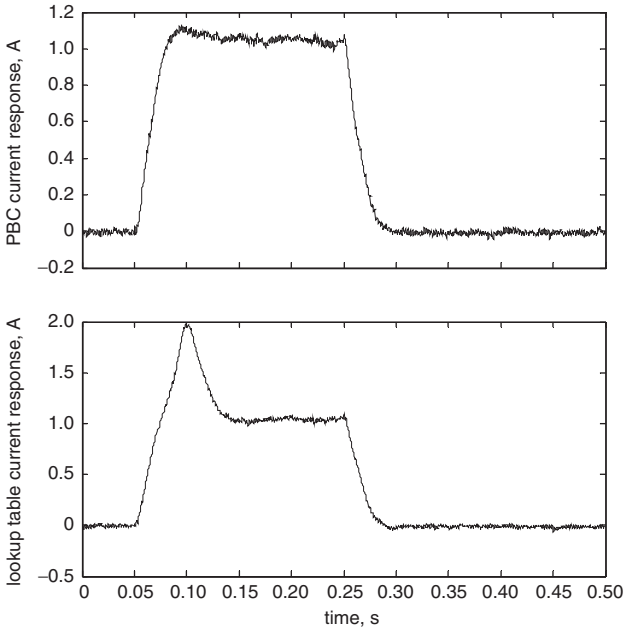

Fig. 9 *Current responses of step flux-linkage input for PBC and lookup table flux-linkage controllers*

9 Conclusion

This paper has described the detailed controller design, simulation and experimental implementation of a PBC controller for the flux regulation of a novel VR finger gripper. The controller can overcome the inherent nonlinear characteristics of the variable reluctance finger gripper and it guarantees the global stability and the asymptotic convergence of all state errors. It also avoids nonlinear system cancellation and enhances the overall system's robustness.

A comprehensive mathematical and PCH model has been constructed. By reshaping the system's natural energy and injecting the required damping, a nonlinear flux controller for the VR finger gripper was developed. Through computer simulation, the proposed control scheme guarantees the global asymptotic stability and system robustness with response to some plant variations and modelling uncertainties.

To confirm the effectiveness of the PBC controller, experimental implementation was carried out. When comparing with the simulation results, it was found that they match closely. The experimental results show that the proposed PBC controller can guarantee global stability, asymptotic convergence and robustness against changes of plant parameters.

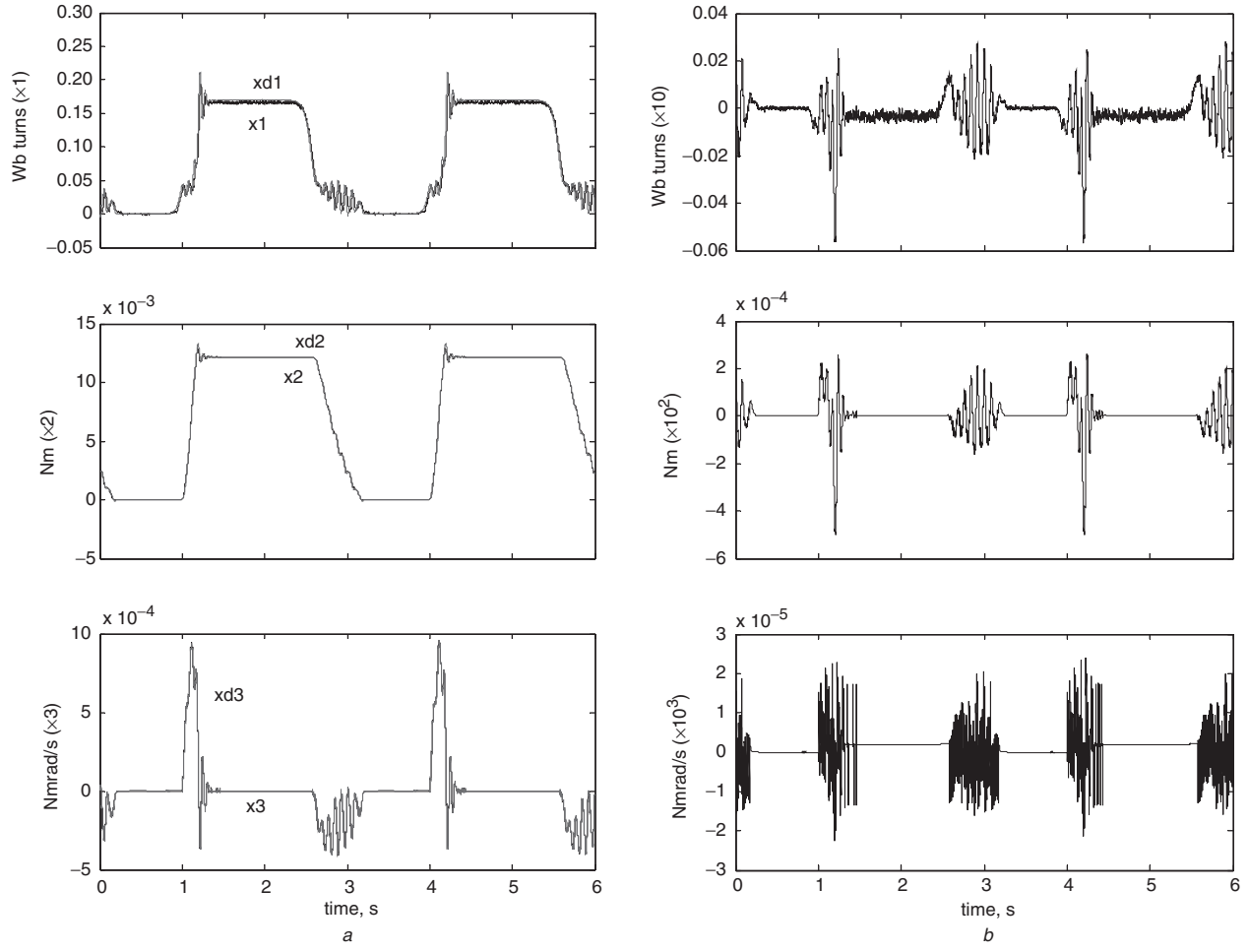

Fig. 10 *Experimental results*
a Tracking responses of each state
b Tracking error of each state

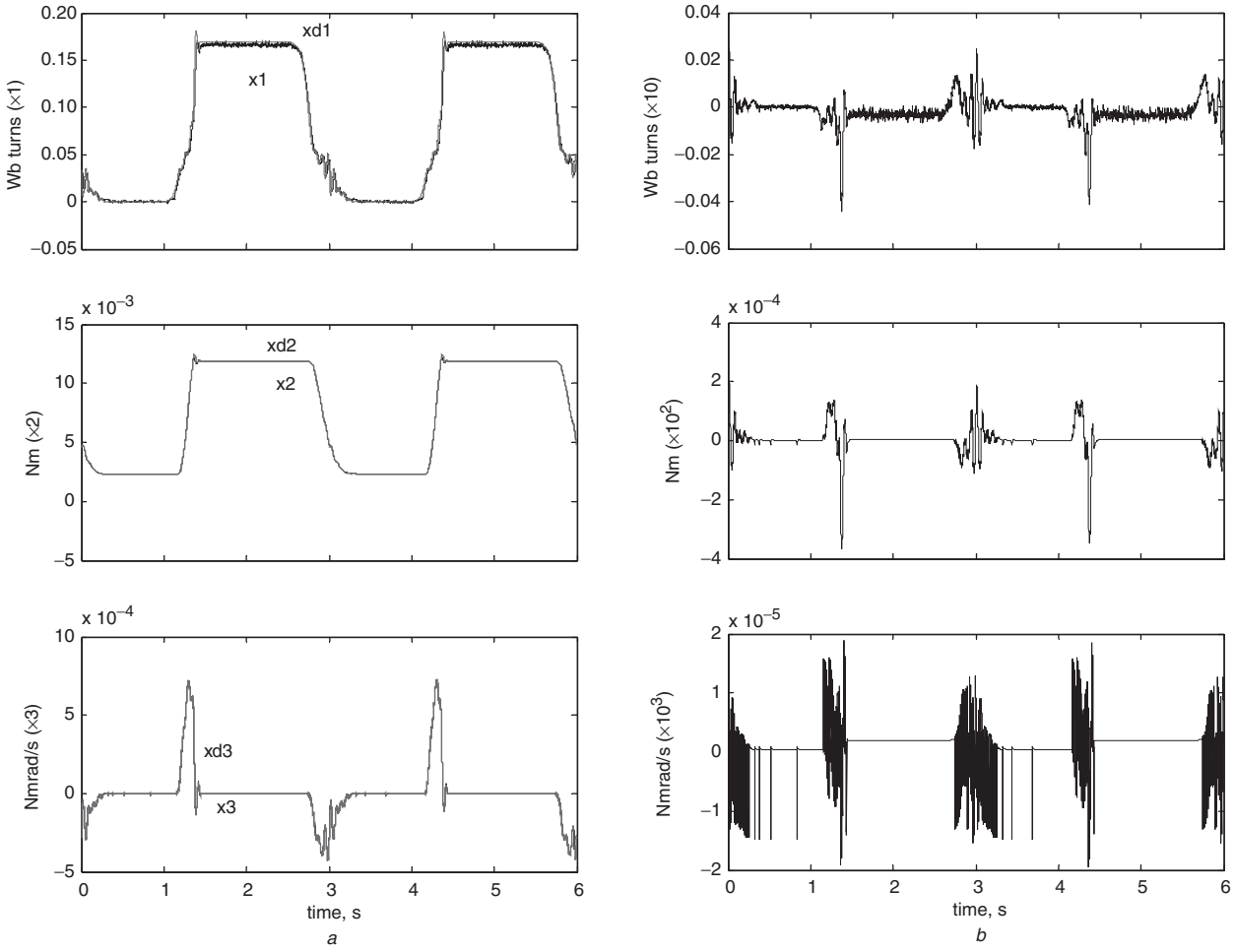

Fig. 11 *Experimental results with spring constant doubled.*
a Tracking responses of each state
b Tracking error of each state

10 Acknowledgment

The authors would like to acknowledge the funding support of the Hong Kong Polytechnic University through research project G-V777 and the general support of South China University of Technology through the Nation Nature Science Fund (China, 60174025).

11 References

1 Miller, T.J.E.: 'Switched reluctance motor and their control' (Magne Physics Publishing and Clarendon Press, Oxford, 1993)
2 Taylor, D.G.: 'An experimental study on composite control of switched reluctance motors', *IEEE Control Syst. Mag.*, 1991, **11**, (2), pp. 31–36
3 Cheung, N.C., and Chan, K.K.-C.: 'PID control of a novel variable reluctance gripper'. Proc. 27th Ann. Conf. of the IEEE Industrial Electronics Society, IECON, Denver, Colorado, USA, 2001, pp. 456–461
4 Rahman, K.M., and Schulz, S.E.: 'High Performance Fully Digital Switched Reluctance Motor Controller for Vehicle Propulsion', *IEEE Trans. Ind. Appl.*, 2002, **38**, (4), pp. 1062–1071
5 Reay, D.S., Mirkazemi-Moud, M., Green, T.C., and Williams, B.W.: 'Switched Reluctance Motor Control via Fuzzy Adaptive Systems', *IEEE Control Syst. Mag.*, 1995, **15**, (3), pp. 8–15
6 Ortega, R., and Van Der Schaft, A.: 'Putting energy back in control', *IEEE Control Syst. Mag.*, 2001, **21**, (2), pp. 18–33
7 Ortega, R., Schaft, A., Maschke, B., and Escobar, G.: 'Energy-shaping of port-controlled Hamiltonian systems by interconnection'. Proc. Conf. on Decision and control, Phoenix, Arizona, USA, 1999, pp. 1646–1651
8 Angulo-Núñez, M.I., and Sira-Ramírez, H.: 'Flatness in the passivity based control of DC-to-DC power converters', Proc. 37th IEEE Conf. on Decision and control, Dec. 1998, Tampa, Florida, USA, pp. 4115–4120
9 Escobar, G., and Sira-Ramírez, H.: 'A passivity based-sliding mode control approach for the regulation of power factor precompensators'. Proc. 37th Conf. on Decision and control, Tampa, Florida, USA, 1998, pp. 2423–2424
10 Ortega, R., and Espinosa, G.: 'Torque regulation of induction motors', *Automatica*, 1993, **29**, (3), pp. 621–633
11 Nagel, N.J., and Lorenz, R.D.: 'Rotating vector methods for smooth torque control of a switched reluctance motor drive', *IEEE Trans. Indust. Appl.*, 2000, **36**, (2), pp. 540–548
12 Tandon, P., Rajarathanam, A. V., and Ehsani, M.: 'Self-tuning control of a switched-reluctance motor drive with shaft position sensor', *IEEE Trans. Ind. Appl.*, 1997, **33**, (4), pp. 1002–1010
13 Franklin, G.F., Powell, J.D., and Emami-Naeini, A.: 'Feedback control of dynamic systems' (Addison Wesley, USA, 1991)
14 Sharma, V.K., Murhty, S.S., and Singh, B.: 'An improved method for the determination of saturation characteristics of switched reluctance motors', *IEEE Trans. Instrum. Meas.*, 1999, **48**, (5), pp. 995–1000